Effect of thermally activated energy on dislocation emission from a blunted crack tip

X. Zeng[1], Q.H. Fang*[1, 2], Y.W. Liu[1]

[1] College of Mechanical and Vehicle Engineering, Hunan University, Changsha, 410082 Hunan Province, PR China
[2] School of Mechanical and Manufacturing Engineering, The University of New South Wales, NSW 2052, Australia
* Corresponding author: Fangqh1327@tom.com

Abstract Thermally activated processes are of fundamental importance for the understanding and modeling of strength of structural materials. The effect of thermally activated on dislocation emission from an elliptically blunted crack tip is investigated. Critical stress intensity factors were simulated for edge dislocation emission from a blunt crack under mode I and mode II loading conditions at high temperature. The results show the impact of thermally activated processes is remarkable, which can affect the value of the critical stress intensity factors for dislocation emission, but doesn't alter the emission angle. The applied electric load will increase with decreasing temperature.

Keywords thermally activated, blunted crack, dislocation emission

1. Introduction

Dislocation emission from a crack tip is one of the most fundamental process for understanding the ductile-brittle behavior in crystalline materials [1]. Once dislocations are emitted, they move out of the crack tip area, leaving behind a dislocation-free zone. An internal back stress due to the dislocations emitted from crack tip accommodates the stress intensity due to applied load, causing an increase in fracture toughness of materials[2]. The previous formulations [3-5] assume the crack tip to be sharp, a situation that is not observed experimentally [6]. However, a real crack in a material is always of finite length and the radius of curvature of the crack tip is never small enough to be zero [7,8]. Physically, an atomically sharp crack will be blunted by one atomic plane. On the other hand, the emission of a dislocation from crack tip results in crack blunting [9,10]. Lung and Wang [11], and Lee [7] calculated the image force on the dislocation near a blunt crack tip. Critical stress intensity factors were developed for edge dislocation emission from a blunt crack [12, 13].

In this paper, we investigated the effect of thermally activated on the emission of edge dislocation from a blunted crack tip. It is also well known that plastic deformation of nanocrystalline and ultrafine-grained metals is thermally activated. Furthermore, thermal activation parameters, such as activation volume and strain-rate sensitivity exponent, strongly depend on grain size and temperature [14-17].When thermally activated deformation processes are to be discussed, the applied stress is generally considered to have two components, i.e.,

$$\tau = \tau_a + \tau^*(T, \dot{\gamma}) \tag{1}$$

where τ is the applied shear stress, τ_a is the long-range internal stress and is athermal in nature. The thermal component τ^* is often called the effective stress and depends on test temperature T and shear strain rate $\dot{\gamma}$. The shear strain rate is formally written as an Arrhenius-type rate equation

[18–21].

$$\dot{\gamma} = \dot{\gamma}_0 \exp\left[-\frac{G(\tau^*)}{kT}\right] \tag{2}$$

where $\dot{\gamma}_0$ is a pre-exponential factor, $G(\tau^*)$ the stress-dependent activation energy for the thermally activated dislocation motion, k the Boltzmann constant.

The present contribution mainly tackles the influence of thermally activated effect on the critical stress intensity factors when dislocation is assumed to be emitted under mode I and mode II loads.

2. Modeling

According to the work of Lubarda [22], the stress fields of an edge dislocation emitted from the surface of the void correspond to the imposed displacement discontinuity along the cut from the surface of the void to the center of the dislocation. As shown in Fig.1, an infinite elastic medium with the elastic properties ν and μ contains a blunted crack (an elliptically hole) of a the radius of curvature $\rho = b^2/a$, where μ is the shear modulus and ν is the Poisson's ratio. The blunted crack is straight and infinitely extended in a direction perpendicular to the xy-plane. Edge dislocation 1 with Burgers vector b_1 was emitted from the surface of the blunted crack to the point $z_0 = a - \rho/2 + r_0 e^{i\theta}$, which represent polar coordinates based on an origin behind the crack root, and edge dislocation 2 with Burgers vector b_2 is located at the surface of crack $z_d = a - \rho/2 + r_d e^{i\theta}$. They are both assumed to be straight and infinite along the direction perpendicular to the xy-plane, and $b_1 = -b_2 = b_x + ib_y = b_r e^{i\theta}$.

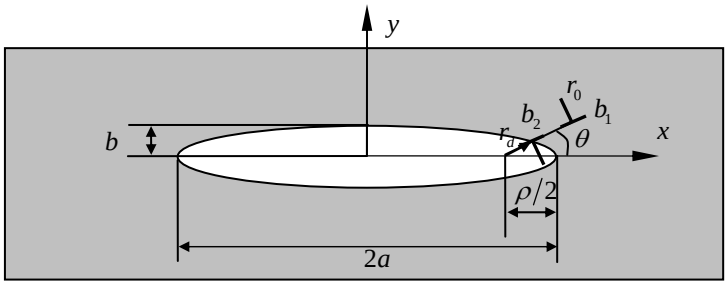

Figure 1 Dislocation emission from an elliptically blunted crack tip.

we first consider only a short range thermal barrier and the associated effective stress component τ^*. The activation energy $G(\tau^*)$ in Eq. (2) is frequently expressed as[20]

$$G(\tau^*) = G_0\left[1-\left(\frac{\tau^*}{\tau_m}\right)^p\right]^q, \quad 0 \le p \le 1, \quad 1 \le q \le 2, \tag{3}$$

where p and q are phenomenological parameters reflecting the shape of a resistance profile,

G_0 is the activation energy and τ_m is the effective stress at 0K . From Eqs. (2) and (3), we have

$$\tau^* = \tau_m \left\{ 1 - \left[\frac{kT \ln(\dot{\varepsilon}_0 / \dot{\varepsilon})}{G_0} \right]^{1/q} \right\}^{1/p} . \tag{4}$$

For given G_0, $\dot{\varepsilon}_0$, p and q, this equation expresses the temperature and strain-rate dependence of the effective stress τ^*.

Now we calculate the effective slip stress τ_m at 0K. According to the work of Nakatani et al.[23], the effective slip stress agrees with Rise's theoretical prediction. We proceed to map conformally the infinite region outside the elliptical hole in the $z = x + iy$ plane to the infinite region outside a circle of a radius R in the $\zeta = \xi + i\eta$ plane through a transformation function

$$z = \omega(\zeta) = \frac{c}{2}\left(\zeta + \frac{1}{\zeta} \right) \tag{5}$$

where $c = \sqrt{a^2 - b^2}$ and $R = \sqrt{(a+b)/(a-b)}$.

The stress fields can be expressed as[ ]

$$\sigma_y + \sigma_x = 2[\varphi'(z) + \overline{\varphi'(z)}] = 2[\varphi'(\zeta)/\omega'(\zeta) + \overline{\varphi'(\zeta)/\omega'(\zeta)}] \tag{6}$$

$$\sigma_y - \sigma_x + 2i\tau_{xy} = 2\left[\bar{z}\varphi''(z) + \psi'(z) \right]$$

$$= 2\left[\overline{\omega(\zeta)} \left[\varphi''(\zeta)\omega'(\zeta) - \varphi'(\zeta)\omega''(\zeta) \right] / \left[\omega'(\zeta) \right]^3 + \psi'(\zeta)/\omega'(\zeta) \right] \tag{7}$$

Using Muskhelishvili's complex potential method [24], the complex potential functions in the $\zeta = \xi + i\eta$ plane can be easily calculated as

$$\varphi(\zeta) = \gamma \ln(\zeta - \zeta_0) - \gamma \ln(\zeta - \zeta_d) - \gamma \ln(\zeta - R^2/\bar{\zeta}_0) + \gamma \ln(\zeta - R^2/\bar{\zeta}_d)$$

$$+ \frac{\bar{a}_0 \bar{\gamma} R^2}{(\zeta - R^2/\bar{\zeta}_0)\bar{\zeta}_0^2} - \frac{\bar{a}_d \bar{\gamma} R^2}{(\zeta - R^2/\bar{\zeta}_d)\bar{\zeta}_d^2} \tag{8}$$

$$\psi(\zeta) = \chi(\zeta) - \frac{\bar{\omega}(R^2/\zeta)}{\omega'(\zeta)}\varphi'(\zeta) \tag{9}$$

$$\chi(\zeta) = \bar{\gamma} \ln(\zeta - \zeta_0) - \bar{\gamma} \ln(\zeta - \zeta_d) - \bar{\gamma} \ln(\zeta - R^2/\bar{\zeta}_0) + \bar{\gamma} \ln(\zeta - R^2/\bar{\zeta}_d)$$

$$+ \frac{a_0 \gamma}{\zeta - \zeta_0} - \frac{a_d \gamma}{\zeta - \zeta_d} \tag{10}$$

where $\gamma = \frac{\mu b_1}{4\pi i(1-\nu)}$, $\zeta_0 = \frac{1}{c}\left(z_0 + \sqrt{z_0^2 - c^2} \right)$, $a_0 = \frac{(R^4 + \zeta_0^2)\zeta_0}{R^2(\zeta_0^2 - 1)} - \frac{\zeta_0^2(\bar{\zeta}_0^2 + 1)}{\bar{\zeta}_0(\zeta_0^2 - 1)}$, $\zeta_d = \frac{1}{c}\left(z_d + \sqrt{z_d^2 - c^2} \right)$,

$$a_d = \frac{(R^4+\zeta_d^2)\zeta_d}{R^2(\zeta_d^2-1)} - \frac{\zeta_d^2(\overline{\zeta}_d^2+1)}{\overline{\zeta}_d(\zeta_d^2-1)}.$$

According to the Peach-Koehler formula[25], and considering Eqs. (6)—(7), we obtain the image force acting on the dislocation

$$\begin{aligned} f_x - if_y &= \left[\hat{\tau}_{xy}(z_0)b_x + \hat{\sigma}_y(z_0)b_y\right] + i\left[\hat{\sigma}_x(z_0)b_x + \hat{\tau}_{xy}(z_0)b_y\right] \\ &= \left(b_y + ib_x\right)\left[\hat{\varphi}'(z_0) + \overline{\hat{\varphi}'(z_0)}\right] + \left(b_y - ib_x\right)\left[\overline{z}_0\hat{\varphi}''(z_0) + \hat{\psi}'(z_0)\right], \end{aligned} \tag{11}$$

where f_x and f_y are the force in the x and y directions, respectively, $\hat{\sigma}_x(z_0)$, $\hat{\sigma}_y(z_0)$ and $\hat{\sigma}_{xy}(z_0)$ are the components of the perturbation stress fields at the dislocation point z_0, $\hat{\varphi}'(z_0)$ and $\hat{\psi}'(z_0)$ are the perturbation complex potentials in the matrix.

According to Qaissaunee and Santare[26], the perturbation complex potentials are calculated as follows:

$$\begin{aligned} \hat{\varphi}'(z_0) = \Bigg[&-\frac{\gamma}{\zeta_0(\zeta_0^2-1)} - \frac{\gamma}{\zeta_0-\zeta_d} - \frac{\gamma}{\zeta_0 - R^2/\overline{\zeta}_0} + \frac{\gamma}{\zeta_0 - R^2/\overline{\zeta}_d} \\ &- \frac{\overline{a}_0\overline{\gamma}R^2}{(\zeta_0\overline{\zeta}_0 - R^2)^2} + \frac{\overline{a}_d\overline{\gamma}R^2}{(\zeta_0\overline{\zeta}_d - R^2)^2}\Bigg] \Big/ \omega'(\zeta_0), \end{aligned} \tag{12}$$

$$\begin{aligned} \hat{\varphi}''(z_0) = \Bigg\{ \Bigg[&\frac{\gamma(2\zeta_0^2-1)}{\zeta_0^4(\zeta_0^2-1)^2} + \frac{\gamma}{(\zeta_0-\zeta_d)^2} + \frac{\gamma}{(\zeta_0 - R^2/\overline{\zeta}_0)^2} - \frac{\gamma}{(\zeta_0 - R^2/\overline{\zeta}_d)^2} \\ &+ \frac{2\overline{\zeta}_0\overline{a}_0\overline{\gamma}R^2}{(\zeta_0\overline{\zeta}_0 - R^2)^3} - \frac{2\overline{\zeta}_d\overline{a}_d\overline{\gamma}R^2}{(\zeta_0\overline{\zeta}_d - R^2)^3}\Bigg] - \frac{c}{\zeta_0^3}\hat{\varphi}'(z_0)\Bigg\} \Big/ \left[\omega'(\zeta_0)\right]^2, \end{aligned} \tag{13}$$

$$\begin{aligned} \hat{\psi}'(z_0) = \Bigg\{ &-\frac{\overline{\gamma}}{\zeta_0-\zeta_d} - \frac{\overline{\gamma}}{\zeta_0 - R^2/\overline{\zeta}_0} + \frac{\overline{\gamma}}{\zeta_0 - R^2/\overline{\zeta}_d} - \frac{\overline{\gamma}}{\zeta_0(\zeta_0^2-1)} + \frac{\gamma\zeta_0^2(\overline{\zeta}_0^2+1)}{\overline{\zeta}_0(\zeta_0^2-1)^3} \\ &+ \frac{a_d\gamma}{(\zeta_0-\zeta_d)^2} - \frac{\gamma(R^4+1)(\zeta_0^3+3\zeta_0)}{R^2(\zeta_0^2-1)^3} - \frac{\zeta_0(\zeta_0^2+R^4)}{R^2(\zeta_0^2-1)}\Bigg[\frac{\gamma}{(\zeta_0-\zeta_d)^2} \\ &+ \frac{\gamma}{(\zeta_0 - R^2/\overline{\zeta}_0)^2} - \frac{\gamma}{(\zeta_0 - R^2/\overline{\zeta}_d)^2} + \frac{2\overline{\zeta}_0\overline{a}_0\overline{\gamma}R^2}{(\zeta_0\overline{\zeta}_0 - R^2)^3} - \frac{2\overline{\zeta}_d\overline{a}_d\overline{\gamma}R^2}{(\zeta_0\overline{\zeta}_d - R^2)^3}\Bigg] \\ &- \frac{\zeta_0^4 - \zeta_0^2R^4 - 3\zeta_0^2 - R^4}{R^2(\zeta_0^2-1)^2}\Bigg[-\frac{\gamma}{\zeta_0-\zeta_d} - \frac{\gamma}{\zeta_0 - R^2/\overline{\zeta}_0} + \frac{\gamma}{\zeta_0 - R^2/\overline{\zeta}_d} \\ &- \frac{\overline{a}_0\overline{\gamma}R^2}{(\zeta_0\overline{\zeta}_0 - R^2)^2} + \frac{\overline{a}_d\overline{\gamma}R^2}{(\zeta_0\overline{\zeta}_d - R^2)^2}\Bigg]\Bigg\} \Big/ \omega'(\zeta_0). \end{aligned} \tag{14}$$

Based on Stagni[27], the primary physical interest lies on the effective slip stress τ_m which are given by

$$\tau_m = \mathrm{Re}\left\{ i\left[\hat{\varphi}'(z_0) + \overline{\hat{\varphi}'(z_0)} \right] - ie^{2i\theta}\left[\overline{z}_0 \hat{\varphi}''(z_0) + \hat{\psi}'(z_0) \right] \right\}. \tag{15}$$

For the linear elastic analysis of plane cases, Creager and Paris's equations [28] can be used to evaluate the stress fields for an elliptically blunted head. So from Creager and Paris's solutions, the in-plane slip stress due to the applied mode I SIF K_{I} and mode II SIF K_{II} is given by

$$\tau_a = \frac{K_{\mathrm{I}}}{2\sqrt{2\pi r_0}} \sin\frac{\theta}{2}\left(1 + \cos\theta + \frac{\rho}{r_0} \right) + \frac{K_{\mathrm{II}}}{\sqrt{2\pi r_0}}\left(\cos\frac{3\theta}{2} + \frac{1}{2}\sin\theta\sin\frac{\theta}{2} - \frac{\rho}{2r_0}\cos\frac{\theta}{2} \right). \tag{16}$$

Combining Eqs. (1), (4), (15) and (16), we obtain the slip stress acting on the dislocation. The equilibrium distance, r_0, at which the total force on the edge dislocation is zero, is given by

$$\frac{K_{\mathrm{I}} \sin\frac{\theta}{2}}{2\sqrt{2\pi r_0}}\left(1 + \cos\theta + \frac{\rho}{r_0} \right) + \frac{K_{\mathrm{II}}}{\sqrt{2\pi r_0}}\left(\cos\frac{3\theta}{2} + \frac{\sin\theta}{2}\sin\frac{\theta}{2} - \frac{\rho\cos\frac{\theta}{2}}{2r_0} \right) + \tau^* = 0 \tag{17}$$

Referencing to the work of Rice and Thomson [1], if the distance between the crack tip and the zero-slip-force position of a dislocation is less than the core radius of dislocation, a new dislocation would be emitted spontaneously from the crack tip. In the present analysis, we assume that the core radius of the dislocation is equal to Burgers vector b_r. Thus, $r_0 = r_d + b_r$, and r_d is expressed by

$$r_d = \frac{\sqrt{a^2 - 0.25a\rho(\sin\theta)^2} - (a - \rho/2)\cos\theta}{\rho(\cos\theta)^2 + a(\sin\theta)^2}\rho. \tag{18}$$

So we obtain the critical applied mode I SIF:

$$K_{\mathrm{I}}^C = -2\sqrt{2\pi r_0}\tau^* \Big/ \sin\frac{\theta}{2}\left(1 + \cos\theta + \frac{\rho}{r_0} \right). \tag{19}$$

Similar to the mode I crack, we have the normalized critical applied mode II SIF:

$$K_{\mathrm{II}}^C = -\sqrt{2\pi r_0}\tau^* \Big/ \left(\cos\frac{3\theta}{2} + \frac{1}{2}\sin\theta\sin\frac{\theta}{2} - \frac{\rho}{2r_0}\cos\frac{\theta}{2} \right). \tag{20}$$

3. Analysis

Utilizing Eqs. (19) and (20), the influence of the surface stress on the critical applied SIFs can be evaluated. Wang et al.[18] examined the temperature dependence of nanocrystalline Ni at a tensile strain rate of $1\times10^{-4}\mathrm{s}^{-1}$. The numerical calculations are presented for a set of thermally activated properties: $p = 0.24$, $q = 1.3$, $\dot{\varepsilon}_0 = 1\times10^{7}\mathrm{s}^{-1}$ and $G_0 = 3.0\mathrm{eV}$ $(4.81\times10^{-19}\mathrm{J})$ (Ni)[29].

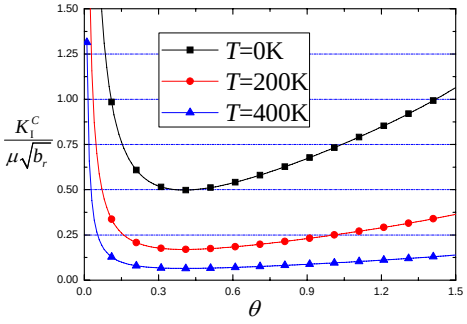

Figure 2 Critical normalized SIF $K_{\mathrm{I}}^{C}/\mu\sqrt{b_r}$ as a function of emission angle θ with different temperature T at $\rho=0.01a$, $a=200b_r$ for nanocrystalline Ni. $T=0$: $K_{\mathrm{I}\min}^{C}/\mu\sqrt{b_r}=0.498$, $\theta_{cr}=0.404$; $T=200$: $K_{\mathrm{I}\min}^{C}/\mu\sqrt{b_r}=0.170$, $\theta_{cr}=0.404$; $T=400$: $K_{\mathrm{I}\min}^{C}/\mu\sqrt{b_r}=0.065$, $\theta_{cr}=0.404$.

For an elliptically blunted crack, the shape can be described by a and the ratio ρ/a. Fig. 2 show the critical normalized SIF for edge dislocation emission as a function of emission angle θ with different temperature T for mode I applied stress ($\rho=0.01a$, $a=200b_r$). The minimum value of $K_{\mathrm{I}}^{C}/\mu\sqrt{b_r}$ indicates the most probable angle θ_{cr} for dislocation emission, and the minimum critical stress and the relative most probable angle for dislocation emission are $K_{\mathrm{I}\min}^{C}/\mu\sqrt{b_r}=0.498$, $\theta_{cr}=0.404$ for $T=0$; $K_{\mathrm{I}\min}^{C}/\mu\sqrt{b_r}=0.170$, $\theta_{cr}=0.404$ for $T=200$; $K_{\mathrm{I}\min}^{C}/\mu\sqrt{b_r}=0.065$, $\theta_{cr}=0.404$ for $T=400$. It is clearly found that the critical SIF decreases from infinity to a minimum and then increases with increasing emission angle θ, which is in agreement with the result in the previous papers[12, 13]. And with the increasing temperature, the minimum value of critical SIF decreases, while the most probable angle for dislocation emission does not change. It means that the high temperature make the dislocation emission take place easily.

The critical normalized SIF $K_{\mathrm{I}}^{C}/\mu\sqrt{b_r}$ as a function of emission angle θ with different crack shape at $T=200\mathrm{K}$ are displayed in Fig. 3(a) and (b). Fig.4(a) and (b) show the critical normalized SIF $K_{\mathrm{I}}^{C}/\mu\sqrt{b_r}$ as a function of temperature T with different crack shape at $\theta=0.5$. They are been seen that the minimum critical SIF and the relative most probable angle are increases with increasing crack length and radius of curvature. And with the increase of temperature, the critical SIF increases, and with the increase in crack length and radius of curvature, the change of the critical load increases.

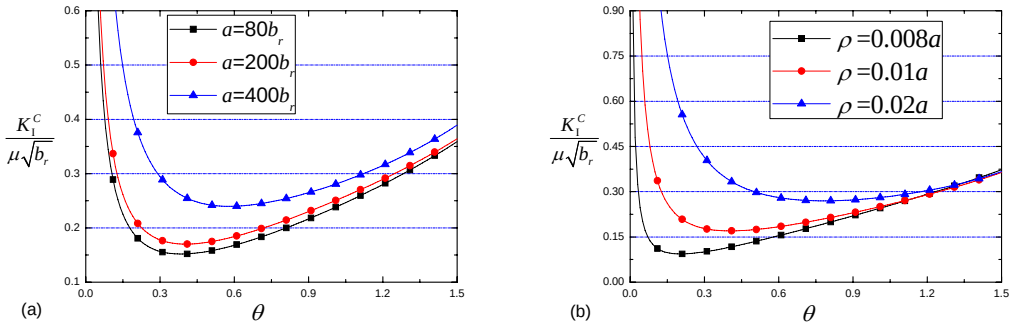

Figure 3 Critical normalized SIF $K_{\mathrm{I}}^{C}/\mu\sqrt{b_r}$ as a function of emission angle θ with different crack shape at $T=200\mathrm{K}$: (a) for $\rho=0.01a$; (b) for $a=200b_r$.

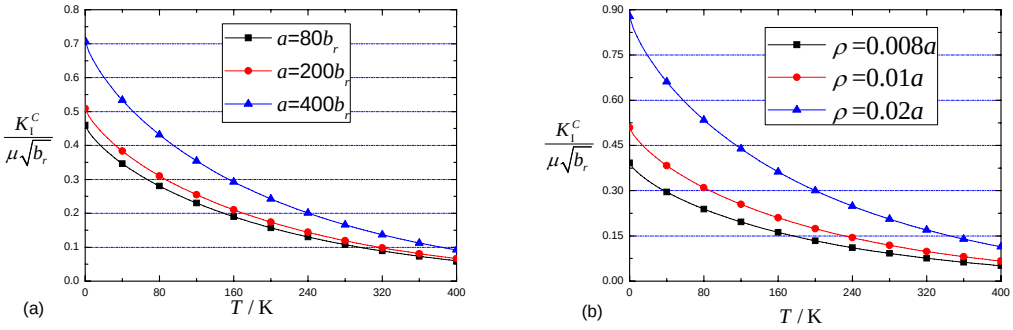

Figure 4 Critical normalized SIF $K_{\mathrm{I}}^{C}/\mu\sqrt{b_r}$ as a function of temperature T with different crack shape at $\theta=0.5$: (a) for $\rho=0.01a$; (b) for $a=200b_r$.

4. Conclusions

The effect of thermally activated on dislocation emission from an elliptically blunted crack tip is investigated. Considering the mechanism that the stress fields of an edge dislocation emitted from the surface of the void correspond to the imposed displacement discontinuity along the cut from the surface of the void to the center of the dislocation, the critical stress intensity factors for edge dislocation emission from a blunt crack under mode I and mode II loading conditions at high temperature were simulated in nanocrystalline and ultrafine-grained metals. The results show the impact of thermally activated processes is remarkable, which can affect the value of the critical stress intensity factors for dislocation emission, but does not alter the emission angle. With the increasing temperature, the minimum value of critical SIF decreases. And the high temperature make the dislocation emission take place easily.

Acknowledgements

The authors would like to deeply appreciate the support from the NNSFC (11172094 and 11172095) and the NCET-11-0122. This work was also supported by Hunan Provincial Natural Science Foundation for Creative Research Groups of China (Grant No.12JJ7001).

References

[1] J.R. Rice, R. Thomson, Ductile versus brittle behaviour of crystals. Philos Mag, 29 (1974) 73-97.

[2] I.H. Lin, R, Thomson, Cleavage, dislocation emission, and shielding for cracks under general loading. Acta Metall, 34 (1986) 187-206

[3] C.C. Huang, C.C. Yu, S. Lee, The behavior of screw dislocations dynamically emitted from the tip of a surface crack during loading and unloading. J Mater Res, 10 (1995) 183-189.

[4] T.C. Wang, Dislocation nucleation and emission from crack tip. Int J Fract, 69 (1995) 295-306.

[5] Y.Z. Tsai, S. Lee, Dynamic emission of screw dislocations from a propagating crack tip. J Appl Phys, 81 (1997) 2089-2093.

[6] J.H. Chen, Q. Wang, G.Z. Wang, Z. Li, Fracture behavior at crack tip—a new framework for cleavage mechanism of steel. Acta Mater, 51 (2003) 1841-1855.

[7] S. Lee, The image force on the screw dislocation around a crack of finite size. Eng Fract Mech, 27 (1987) 539-545.

[8] B.T. Chen, T.Y. Zhang, S. Lee, Interaction of an edge dislocation with an elliptical hole in a rectilinearly anisotropic body. Mech Mater, 31 (1999) 71-93.

[9] S.M. Ohr, An electron microscopy study of crack tip deformation and its impact on dislocation theory of fracture. Mater Sci Eng, 72 (1985) 1-35.

[10] S.J. Zhou, A.E. Carlsson, R. Thomson, Crack blunting effects on dislocation emission from cracks. Phys Rev Lett, 72 (1994) 852-855.

[11] C.W. Lung, L.Wang, The image force on the dislocation near a finite length crack tip. Philos Mag, 50 (1984) L91-L24.

[12] M. Huang, Z. Li, Dislocation emission criterion from a blunt crack tip. J Mech Phys Solids, 52 (2004) 1991-2003.

[13] Q.H. Fang, Y. Liu, Y.W. Liu, B.Y. Huang, Dislocation emission from an elliptically blunted crack tip with surface effects. Physica B 404 (2009) 3421-3424.

[14] Y.M.Wang, E. Ma, Strain hardening, strain rate sensitivity, and ductility of nanostructured metals. Mater Sci Eng A, 375 – 377 (2004) 46-52.

[15] Q.Wei, S. Cheng, K.T. Ramesh, E. Ma, Effect of nanocrystalline and ultrafine grain sizes on the strain rate sensitivity and activation volume: fcc versus bcc metals. Mater Sci Eng A, 381 (2004) 71-79.

[16] R.W. Hayes, D. Witkin, F. Zhou, E.J. Lavernia, Deformation and activation volumes of cryomilled ultrafine-grained aluminum. Acta Mater, 52 (2004) 4259-4271.

[17] Y.J. Li, X.H. Zeng,W. Blum, Transition from strengthening to softening by grain boundaries in ultrafine-grained Cu. Acta Mater, 52 (2004) 5009-5018.

[18] Y.M.Wang, A.V. Hamza, E. Ma, Temperature-dependent strain rate sensitivity and activation volume of nanocrystalline Ni. Acta Mater, 54 (2006) 2715 – 2726.

[19] H. Conrad, Thermally activated deformation of metals. J Metals, 16 (1964) 582-588.

[20] U.F. Kocks, A.S. Argon, M.F. Ashby, Thermo-dynamics and Kinetics of Slip. Prog Mater Sci, 19 (1975) 1 – 278.

[21] M. Dao, L. Lu, R.J. Asaro, J.T.M. De Hosson, E. Ma, Toward a quantitative understanding of mechanical behavior of nanocrystalline metals. Acta Mater, 55 (2007) 4041-4065.

[22] V.A. Lubarda, Image force on a straight dislocation emitted from a cylindrical void. Int J Solids

Struct, 48 (2011) 648-660.

[23] A. Nakatani, H. Kitagawa, Y. Shibutani, K. Nakatani, Molecular dynamics study on ductile crack process effect of temperature on dislocation nucleation. Mater Sci Res Int, 1 (1995) 11-16.

[24] NI. Muskhelishvili, Some basic problems of the mathematical theory of elasticity, Noordhoff International Publishing, Leyden 1975.

[25] J.P. Hirth, J. Lothe, Theory of Dislocations, 1982, 2nd edn. (John Wiley, New York).

[26] M.T. Qaissaunee, M.H. Santare, Edge dislocation interacting with an elliptical inclusion surrounded by an interfacial zone. Q J Mech Appl Math, 48 (1995) 465-482.

[27]L. Stagni, Edge dislocation near an elliptic inhomogeneity with either an adhering or a slipping interface - A comparative study. Phil Mag A, 68(1993) 49-57.

[28] M. Creager, P.C. Paris, Elastic field equations for blunt cracks with reference
to stress corrosion cracking. Int J Fract Mech, 3 (1967) 247-252.

[29] L. Hollang, E. Hieckmann, D. Brunner, C. Holste, W. Skrotzki, Scaling effects in the plasticity of nickel. Mater Sci Eng A, 424 (2006) 138 – 153.